ACS APPLIED MATERIALS & INTERFACES

Research Article

www.acsami.org

Laser-Modified Black Titanium Oxide Nanospheres and Their Photocatalytic Activities under Visible Light

Xing Chen,[†] Dongxu Zhao,*[,†] Kewei Liu,[†] Chunrui Wang,[‡] Lei Liu,*[,†] Binghui Li,[†] Zhenzhong Zhang,[†] and Dezhen Shen*[,†]

[†]State Key Laboratory of Luminescence and Applications and [‡]State Key Laboratory of Laser Interaction with Matter, Changchun Institute of Optics, Fine Mechanics and Physics, Chinese Academy of Sciences, 3888 Dongnanhu Road, Changchun 130021, PR China

Supporting Information

ABSTRACT: A facile pulse laser ablation approach for preparing black titanium oxide nanospheres, which could be used as photocatalysts under visible light, is proposed. The black titanium oxide nanospheres are prepared by pulsed-laser irradiation of pure titanium oxide in suspended aqueous solution. The crystalline phases, morphology, and optical properties of the obtained nanospheres are characterized by means of X-ray diffraction (XRD), field-emission scanning electron microscopy (SEM), transmission electron microscopy (TEM), selected area electron diffraction (SAED), X-ray photoelectron spectroscopy (XPS), and UV−vis−NIR diffuse reflectance spectroscopy. It is shown that high-energy laser ablation of titanium oxide suspended solution benefited the formation of Ti^{3+} species and surface disorder on the surface of the titanium oxide nanospheres. The laser-modified black titanium oxide nanospheres could absorb the full spectrum of visible light, thus exhibiting good photocatalytic performance under visible light.

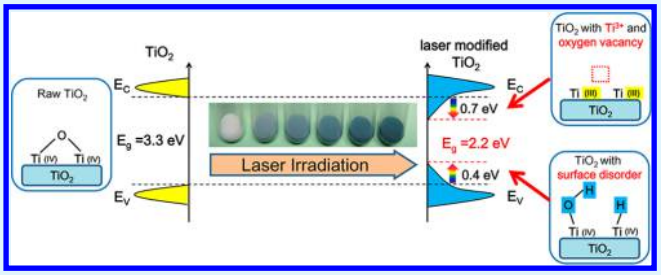

KEYWORDS: *titanium oxides, laser, nanospheres, visible light, photocatalytic*

1. INTRODUCTION

Titanium dioxide (TiO_2) has attracted extensive interest because it was found to be an efficient photocatalyst by Honda and Fujishima.[1] At present, TiO_2 has become the most promising candidate for photoelectrochemical water splitting,[2−4] organic pollutant degradation,[5−7] dye-sensitized solar cells,[8,9] and other photocatalytic applications[10−14] because of its low cost, good chemical stability, and nontoxicity.[15] However, pure TiO_2 with its relatively large band gap (3.0 and 3.2 eV for rutile and anatase phases, respectively) can be activated only by ultraviolet (UV) light, which represents a small fraction of solar spectrum.

To overcome this drawback, pure TiO_2 has been modified by impurity doping and dye sensitization. In impurity doping, the chemical composition of TiO_2 is varied by adding transitional metals,[16−18] noble metals,[19,20] or nonmetals,[21−24] which could generate donor or acceptor states in the band gap. The doping of TiO_2, despite being the most common approach to improving visible light absorption characteristics of TiO_2, has many disadvantages. For example, these doped TiO_2 catalysts have the drawbacks of secondary phase and the introduction of impurities strongly affecting the lifetime of the e−h pair.[11] In dye sensitization, organic molecules coated on the TiO_2 surface were used to absorb visible light, and then an electron was injected from the excited state of the dye molecule into the conduction band of the semiconductor.[25,26] However, the dye degraded itself through the photocatalytic degradation of organic pollutants. As an alternative to organic dyes, metallic nanostructures have been successfully used as photosensitizers,[27] but it was difficult to produce metallic nanostructure sensitizers with the advantages of finely tunable structure, mechanical durability, and low cost.

In recent years, an alternative approach has been developed to improve the visible and infrared optical absorption by engineering disorder states in TiO_2.[28−35] A porous TiO_2 nanocrystal was prepared followed by the hydrogenation to create a disordered layer on the nanocrystal surface. The disorder-engineered TiO_2 nanocrystals exhibited substantial solar-driven photocatalytic activities.[28] Several methods were developed to prepare hydrogenated black TiO_2, such as thermal treatments under a hydrogen atmosphere[31−33] and treatment by hydrogen plasma.[34,35] Fan et al. have developed a simple one-step combustion method to synthesize Ti^{3+}-doped TiO_2. The partially reduced TiO_2, which contains Ti^{3+} or oxygen vacancy, has been demonstrated to exhibit visible light absorption.[29]

Here, we proposed facile laser-modified TiO_2 nanospheres that could be used as photocatalysts under visible light to degrade organic pollutants. The TiO_2 nanoparticles were irradiated by a pulsed laser to form TiO_2 nanosphere

Received: May 26, 2015
Accepted: July 1, 2015
Published: July 1, 2015

DOI: 10.1021/acsami.5b04568
ACS Appl. Mater. Interfaces 2015, 7, 16070−16077

morphology. The Ti^{3+} species and disorder was introduced to the surface of the TiO_2 nanospheres. The laser-modified TiO_2 nanospheres could absorb visible and infrared light and had photocatalytic activities under visible light.

2. EXPERIMENTAL SECTION

2.1. Preparation of TiO_2 Nanospheres. In a typical reaction, 20 mg of TiO_2 (Aldrich, anatase, 100 nm) was added into 1 mL of distilled water followed by ultrasonic treatment for 10 min to form a suspension. The suspended solution was transferred into a cuvette. A Nd:YAG pulsed laser (Continuum PRII-8000, λ = 355 nm, pulse duration = 8 ns, frequency = 10 Hz, power = 0.35 W, instantaneous power = 4.4 MW) was irradiated onto one side of the cuvette for several minutes, then the laser was irradiated onto the other side of the cuvette for the same time. The total duration of laser irradiation was n minutes. The laser beam gave a circular and homogeneous spot, which allowed a 0.7 cm^2 area to be treated. The experimental setup is schematically shown in Figure 1.

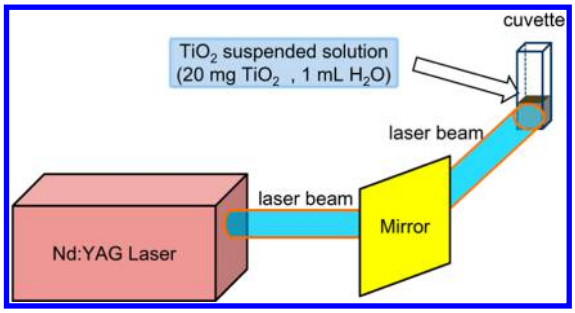

Figure 1. Schematic of the experimental setup.

After laser irradiation, the TiO_2 was filtered and dried at 80 °C for 12 h. The prepared samples were designated as TiO_2-n (the duration of laser irradiation was n minutes, n = 5, 15, 30, 60, and 120). All chemicals were analytical-grade and were used as received without further purification.

2.2. Characterization. To determine the crystal phase composition of samples, X-ray diffraction (XRD) measurements were carried out at room temperature using a Rigaku D/max-RA X-ray spectrometer with Cu Kα radiation (λ = 0.15418 nm). An accelerating voltage of 40 kV and an emission current of 40 mA were used.

The morphology and structure properties of samples were investigated by field-emission scanning electron microscopy (FESEM, Hitachi S-4800). Samples for SEM observation were prepared by dispersing the prepared samples in alcohol, followed by ultrasonic treatment. A small portion of the suspended solution was dropped onto a smooth silicon slice. After being dried at 110 °C for 4 h, the silicon slice was adhered on an aluminum mount by an adhesive conductive-carbon paper.

The microstructures of the samples were examined by transmission electron microscopy (TEM) on a JEOL JEM-2100F electron microscope. Samples for TEM observation were prepared by dispersing the prepared samples in alcohol, followed by ultrasonic treatment. A small portion of the suspended solution was dropped onto a copper grid, and then the copper grid was dried at 60 °C for 12 h.

The core levels and valence band X-ray photoelectron spectra (XPS) were measured with an ESCALAB Mk II (Vacuum Generators) spectrometer using Al Kα X-rays (240 W). The binding energies were calibrated against the C 1s signal (284.6 eV) of adventitious carbon.

The UV−vis−NIR diffuse reflectance spectra were recorded on a Shimadzu UV-3101PC UV−vis−NIR spectrophotometer operating in the diffuse mode.

2.3. Photocatalytic Reaction. The photocatalytic activity of prepared TiO_2 nanospheres was measured by monitoring the change in optical absorption of a rhodamine B solution at 553 nm during its photocatalytic decomposition process. In a typical experiment, 5 mg of TiO_2 nanospheres was added to 15 mL of rhodamine B solution that had an optical absorption of approximately 2.0 at 553 nm. The suspended solution was magnetically stirred in the dark for 1 h and then exposed to green light from a green LED (voltage = 3.7 V, current = 25 mA, and center wavelength = 520 nm). We also tested the photocatalytic activity under irradiation of a red LED (voltage = 2.0 V, current = 45 mA, and center wavelength = 676 nm). The luminescent spectrum of the LED was shown in Figure S1 (Supporting Information). For a given time interval, the suspended solution was centrifuged, and then the filtrates were analyzed. The concentration of rhodamine B was monitored by the optical absorption peak by a Shimadzu UV3101PC UV−vis−NIR spectrophotometer.

3. RESULTS AND DISCUSSION

3.1. Morphology and Structure Properties of TiO_2 Nanospheres. As shown in Figure 2, it could be seen that

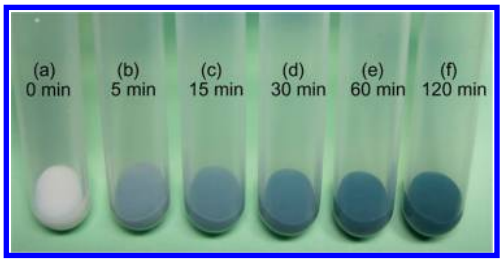

Figure 2. Suspended TiO_2 solution before and after laser modification. (a) raw TiO_2, (b) TiO_2-5, (c) TiO_2-15, (d) TiO_2-30, (e) TiO_2-60, and (f) TiO_2-120.

the color of the suspended TiO_2 solution changed from white to gray after laser irradiation for only 5 min. As the duration of the laser modification increased, the color of the suspended TiO_2 solution became deeper, turning totally became black after laser irradiation for 120 min. After the laser irradiation, the TiO_2 powder was filtered and dried. The photos of unmodified TiO_2 and laser-modified black TiO_2 powder are shown in Figure 3. The color of TiO_2 powder changes from white to

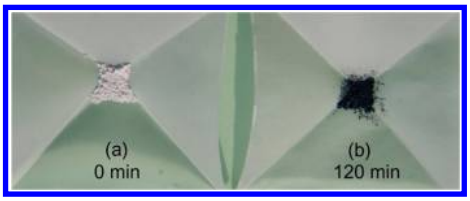

Figure 3. TiO_2 powder before and after laser modification. (a) Raw TiO_2 and (b) TiO_2-120.

black after laser modification for 120 min, which suggests that the visible light could be totally absorbed by the laser-modified black TiO_2.

The structure of the TiO_2 powders before and after the laser modification were explored by XRD. XRD revealed the structure of the mixture of the laser-induced TiO_2 nanospheres and unreacted raw TiO_2. The powder XRD patterns of TiO_2 synthesized under different durations of laser irradiation are shown in Figure 4. For the sample before laser irradiation, the XRD pattern is composed of lines at 25.3, 36.9, 37.8, 38.6, 48.1, 53.8, and 55.2°, corresponding to (101), (103), (004), (112), (200), (105), and (211) lattice plane reflections of the anatase TiO_2 phase (Powder Diffraction File (PDF) no. 21-1272, International Centre for Diffraction Data (ICDD), 1990), respectively. There are no other diffraction peaks except the

DOI: 10.1021/acsami.5b04568
ACS Appl. Mater. Interfaces 2015, 7, 16070−16077

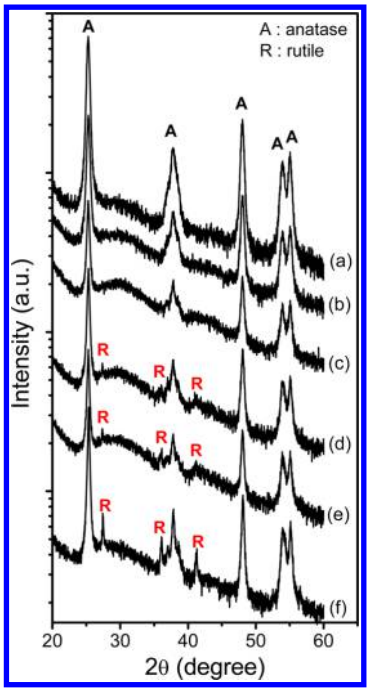

Figure 4. XRD patterns of TiO_2 before and after laser modification (2θ range from 20 to 60°). (a) Raw TiO_2, (b) TiO_2-5, (c) TiO_2-15, (d) TiO_2-30, (e) TiO_2-60, and (f) TiO_2-120.

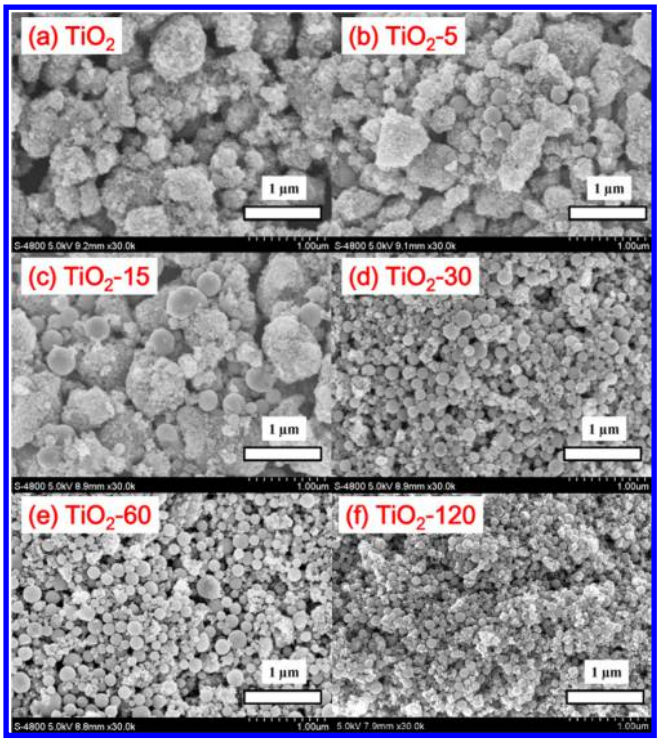

Figure 5. SEM images of TiO_2 before and after laser modification: (a) raw TiO_2, (b) TiO_2-5, (c) TiO_2-15, (d) TiO_2-30, (e) TiO_2-60, and (f) TiO_2-120.

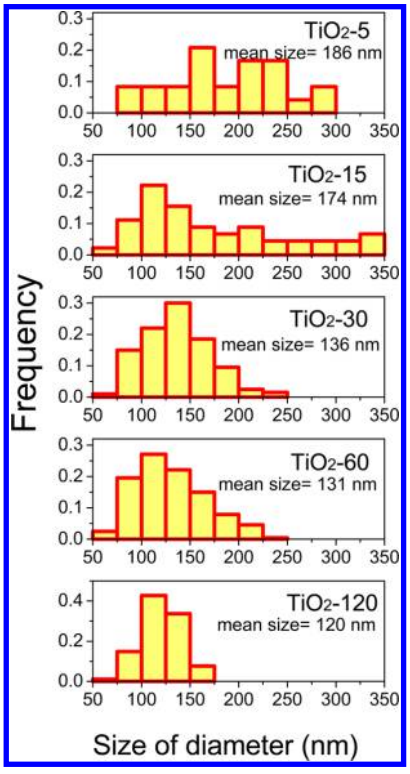

Figure 6. Size histogram of TiO_2 nanospheres.

diffraction peaks of anatase TiO_2 when the duration of laser irradiation was less than 15 min. When the laser irradiation duration lasts 30 min, three new diffraction peaks located at 27.4, 36.1, and 41.3° appear, corresponding to (110), (101), and (111) lattice plane reflections of the rutile TiO_2 phase (PDF no. 21-1276, ICDD, 1990). The diffraction peaks of rutile TiO_2 phase increase as the duration of laser modification increases. The results of XRD suggest that the anatase phase TiO_2 tends to transform to rutile phase under relatively long durations of laser modification because the rutile phase is more stable under high temperature and high pressure caused by pulsed-laser irradiation.

Figure 5 shows the SEM images of the TiO_2 powders before and after the laser modification. It could be seen that TiO_2 nanospheres appear after laser irradiation for only 5 min. By increasing the laser irradiated time, the amount of TiO_2 nanospheres increases. A summary of statistics on the size of the obtained TiO_2 nanospheres is shown in Figure 6. (The statistics on the size of the raw TiO_2 are shown in Figure S2.)

The average size of TiO_2 nanospheres is about 180 nm for the samples of TiO_2-5 and TiO_2-15. As the duration of laser irradiation increases, the average size decreases from 180 to approximately 130 nm. The size distribution of TiO_2 nanospheres is relatively broad for the samples of TiO_2-5 and TiO_2-15, and the size distribution of TiO_2 nanospheres becomes narrow for the samples of TiO_2-30, TiO_2-60, and TiO_2-120.

The results of SEM suggest that the TiO_2 nanospheres are produced by the laser ablation of TiO_2 nanoparticles. The initial TiO_2 nanospheres have relatively large diameters and a broad size distribution. When irradiated by laser for a long duration, the initial TiO_2 nanospheres continue to be ablated and to form relatively small TiO_2 nanospheres, which have a narrow size distribution. Although the duration is prolonged from 30 to 120 min, the mean size of TiO_2 nanospheres decreases only a little, which means the mean size around 120–130 nm is probably a stable condition under a relatively long duration of laser irradiation in our experimental conditions.

3.2. Optical Properties of TiO_2 Nanospheres. To carry out a more complete characterization of light absorption,

DOI: 10.1021/acsami.5b04568
ACS Appl. Mater. Interfaces 2015, 7, 16070–16077

several UV−vis diffuse reflectance spectra of raw and laser irradiated TiO_2 were carried out. The results are shown in Figure 7. Figure 7a shows the diffuse reflectance data that is

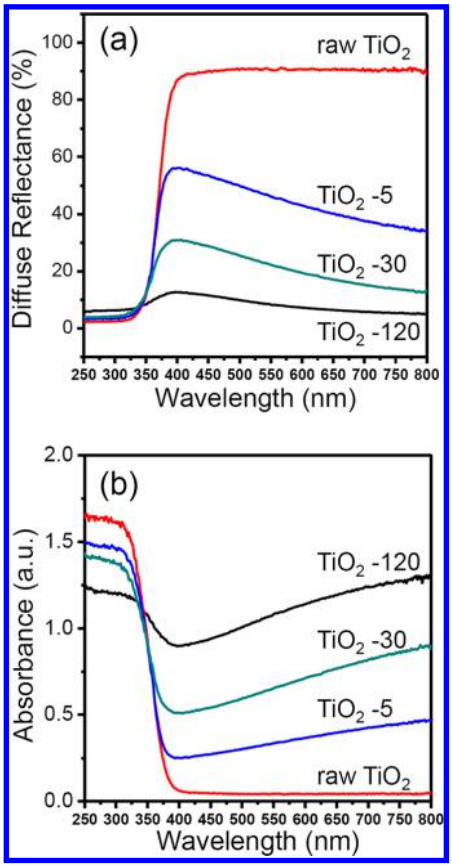

Figure 7. UV−vis diffuse reflectance spectra of TiO_2 before and after laser modification: (a) diffuse reflectance data and (b) absorbance data ($A = \log(1/R)$, A for absorbance and R for diffuse reflectance).

measured directly, and Figure 7b shows absorbance data that is calculated by the formula $A = \log(1/R)$ (A for absorbance and R for diffuse reflectance). After laser modification, being compared with the raw white TiO_2 with an absorption edge of ca. 400 nm, the absorption of the laser-modified TiO_2 powders could extend to the full visible light spectrum and up to the near-infrared spectrum of 2000 nm. (UV−vis−NIR diffuse reflectance spectra are shown in Figure S3 in Supporting Information.) Meanwhile, the absorption above the wavelength of 400 nm increases as the duration of laser irradiation increasing.

The band gap values of samples are determined according to Kubelka−Munk function method as shown in Figure 8. The band gap of the laser irradiation TiO_2 shifts from 3.3 to 2.2 eV. Moreover, an enhanced absorption for photon energy below the 2.2 eV has been observed in our UV−visible spectra. It was reported that high concentration of oxygen vacancy could break the selection rule for indirect transitions of TiO_2 and enhanced absorption for photon energy below the direct band gap.[29] Furthermore, Ti^{3+} and oxygen vacancy could be induced in TiO_2 by high-energy particle bombardment.[36] In our case, it is probably due to the laser irradiation that the high concentration of Ti^{3+} and oxygen vacancy are generated on the surface of TiO_2 resulting in an enhanced absorption for photon energy

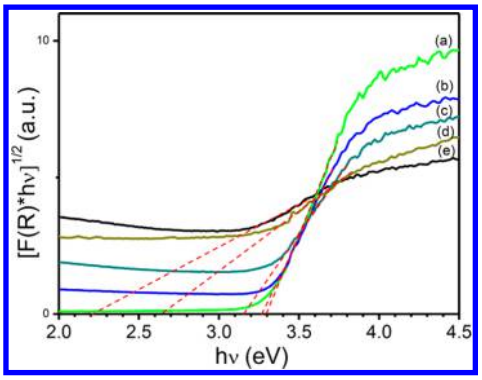

Figure 8. Plots of $[F(R)*h\nu]^{1/2}$ vs the energy of light for TiO_2 before and after laser modification: (a) raw TiO_2, (b) TiO_2-5, (c) TiO_2-30, (d) TiO_2-60, and (e) TiO_2-120. $F(R)$ is the Kubelka−Munk function, and $F(R) = (1-R)^2/2R$.

below the direct band gap. The exits of Ti^{3+} and oxygen vacancy are confirmed by the characterization of XPS.

3.3. Photocatalytic Performance of TiO_2 Nanospheres under Visible Light. The optical properties suggest that laser-modified TiO_2 nanospheres have the potential to act as a photocatalyst under visible light. Rhodamine B is a kind of organic dye, which is often used as a model pollutant to study the photocatalytic activity of photocatalysts. Here, we used rhodamine B as a model pollutant to study the photocatalytic activity of TiO_2 before and after laser modification. When the mixed solution of rhodamine B and TiO_2 was exposed to the green light irradiation from a LED at room temperature, it was found that the absorptive intensity of rhodamine B at 553 nm decreased as light irradiation time increased. We also found that the absorptive intensity of rhodamine B at 553 nm even decreased in the dark for 5 h. It was due to this that the adsorption equilibrium of rhodamine B with the catalyst cannot be completely reached in only 1 hour in a dark environment. To analyze the actual degradation ratio of rhodamine B, we calculated the $\Delta C/C_0$ on the basis of the formula $\Delta C/C_0 = (C/C_0)_{dark} - (C/C_0)_{light}$. The results are shown in Figure 9. (The data of $(C/C_0)_{dark}$ and $(C/C_0)_{light}$ are shown in Figures S4 and S5 in the Supporting Information, respectively). The $\Delta C/C_0$ is approximately constant at 0 when using P25 or pure TiO_2 as catalysts, indicating that P25 and pure TiO_2 cannot degraded rhodamine B under visible light. The $\Delta C/C_0$ of laser-modified TiO_2 nanospheres increases as light irradiation time increases,

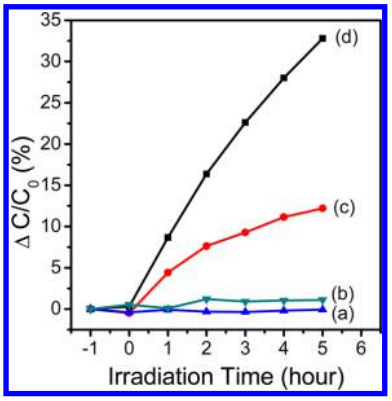

Figure 9. Photocatalytic degradation curves of rhodamine B under irradiation of green LED ($\Delta C/C_0$ vs irradiation time): (a) P25, (b) raw TiO_2, (c) TiO_2-60, and (d) TiO_2-120.

DOI: 10.1021/acsami.5b04568
ACS Appl. Mater. Interfaces 2015, 7, 16070−16077

and the degradation ratio of rhodamine B could be up to 33% after irradiation with green light for 5 h when using TiO_2-120 as catalyst. The sample of TiO_2-120, which was irradiated by pulsed laser for 120 min, has strong absorption in the isible and infrared light region, which is in good agreement with the activity for photocatalytic degradation of organic pollutants in this region. Light absorption is a necessary condition for the photocatalyst to be functional. The photocatalytic activity of TiO_2-120 is higher than that of TiO_2-60 because of the higher visible light absorption ability of TiO_2-120. We also tested the photocatalytic activity of the TiO_2-120 under irradiation from a red LED. The results are shown in Figure 10. It is found that

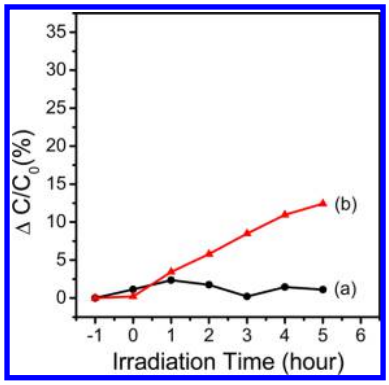

Figure 10. Photocatalytic degradation curves of rhodamine B under irradiation of red LED ($\Delta C/C_0$ vs irradiation time): (a) P25 and (b) TiO_2-120.

P25 cannot degrade rhodamine B under red light either. In contrast, the degradation ratio of rhodamine B could be up to 12% after irradiation by red light for 5 h when using TiO_2-120 as catalyst, and the photocatalytic activity of TiO_2-120 reveals a different intensity under green light and red light. This is probably due to the different light absorption ability. The energy of green light (center wavelength is 520 nm) is higher than the band gap of TiO_2-120 (2.2 eV, corresponding to a light wavelength of 564 nm). Therefore, TiO_2-120 could absorb green light intensely, and e^-—h^+ pairs could be produced effectively. For the red light (center wavelength is 676 nm), even though its energy is lower than the band gap, it could also be absorbed by TiO_2-120, but it would be harder to produce e^-—h^+ pairs effectively.

3.4. Surface States of TiO_2 Nanospheres. The TEM and selected-area electron-diffraction (SAED) patterns of laser-modified TiO_2 are shown in Figure 11. The TEM and SAED for TiO_2-5 reveal an amorphous nature of particles. In the TEM image of TiO_2-30, we could determine fringe separations of 0.218 nm, which corresponds to {111} rutile TiO_2 crystal planes. The SAED pattern of TiO_2-30 is a group of concentric rings, indicating that the TiO_2 nanospheres were polycrystals. To investigate the crystalline phases of the TiO_2 nanospheres, a careful analysis of the SAED patterns was carried out (shown in Figure S6 in Supporting Information). Most interplanar distances could be assigned to various family planes of anatase and rutile phases. The distances of 0.351 and 0.162 nm are in agreement with {101} and {211} family planes of anatase TiO_2, respectively. The distances of 0.310, 0.241, and 0.211 nm are in agreement with {110}, {101}, and {111} family planes of rutile TiO_2, respectively. Thus, there are at least two crystalline phases coexisting in the ablated nanospheres. In the TEM image of TiO_2-120, we could determine the fringe separations of 0.248 nm, which corresponds to {101} rutile TiO_2 crystal planes. The SAED for TiO_2-120 reveals an almost single-crystal morphology.

We also find some defects and disorder in the TEM images of TiO_2-30 and TiO_2-120 that are outlined by dashed circles in Figure 11. The introduction of disorder at their surface would enhance visible and infrared absorption, with the additional benefit of carrier trapping.[28] This enhancement was probably the reason for the color change of the laser-modified TiO_2 nanospheres. Large amounts of lattice disorder in semiconductors could yield midgap states, which can form a continuum extending to and overlapping with the conduction band edge, known as band tail states. Similarly, large amounts of disorder can result in band tail states merging with the valence band.[36,37]

To investigate the change of the surface chemical bonding of TiO_2 nanocrystals induced by the laser irradiation, XPS analysis

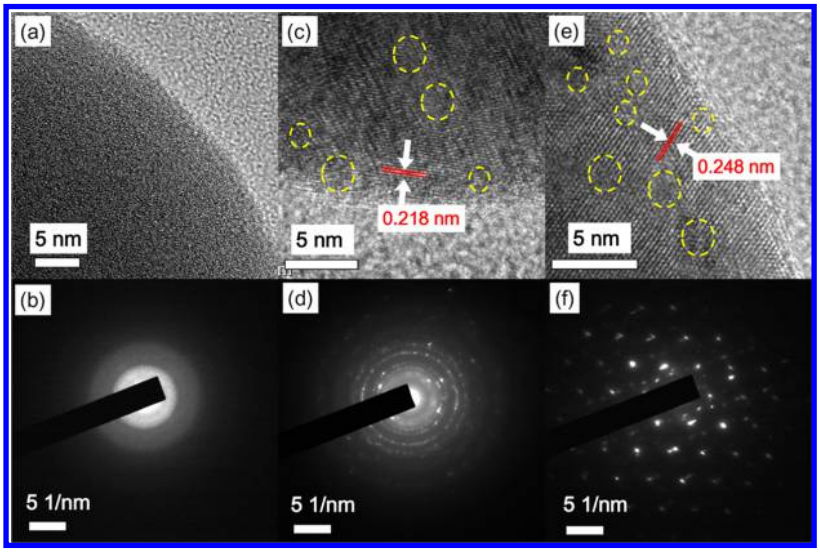

Figure 11. TEM images and SAED patterns of laser-modified TiO_2: (a and b) TiO_2-5, (c and d) TiO_2-30, and (e and f) TiO_2-120. In c and e, dashed circles were applied to outline the disorder regions.

DOI: 10.1021/acsami.5b04568
ACS Appl. Mater. Interfaces 2015, 7, 16070−16077

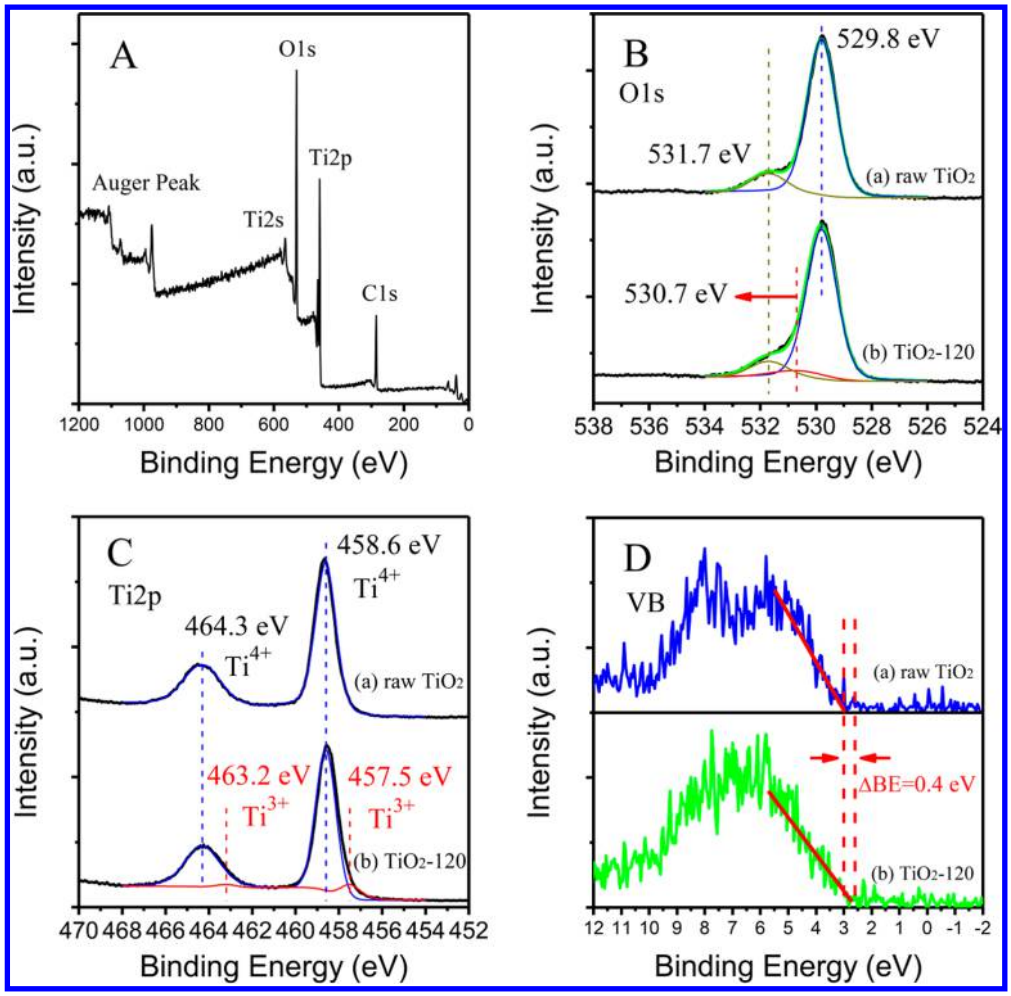

Figure 12. (A) XPS spectrum of TiO_2-120. (B) O 1s XPS spectra of raw TiO_2 and TiO_2-120. (C) Ti 2p XPS spectra of raw TiO_2 and TiO_2-120. (D) Valence band XPS spectra of raw TiO_2 and TiO_2-120.

of raw TiO_2 and TiO_2-120 were carried out. On the basis of the survey XPS spectrum of TiO_2-120 (Figure 12A), the surface of TiO_2-120 is clean except for trace impurities of carbon. The O 1s spectra are shown in Figure 12B. The spectra are fitted with the nonlinear least-squares fit program using Gauss−Lorentz peak shapes. The spectra of raw TiO_2 and TiO_2-120 could be decomposed into a superposition of two and three peaks, respectively. For raw TiO_2, these peaks are attributed to lattice oxygen of TiO_2 (529.8 eV) and adsorbed O_2 (531.7 eV). In contrast, a new peak (530.7 eV) appears in the spectrum of TiO_2-120, which is attributed to Ti−OH species (surface disorder of TiO_2). The details of the parameters of the O 1s peak are shown in Table S1 in the Supporting Information.

The XPS spectra of Ti 2p are shown in Figure 12C. The peaks located at 458.6 and 464.3 eV are assigned to Ti^{4+} $2p_{3/2}$ and Ti^{4+} $2p_{1/2}$, respectively. For TiO_2-120, two new peaks appear. These peaks could be attributed to Ti^{3+} $2p_{3/2}$ (457.5 eV) and Ti^{3+} $2p_{1/2}$ (463.2 eV), respectively. The Ti^{3+} peak areas account for 12% of the total areas of Ti 2p, which means that 12% of Ti ions are Ti^{3+} ions. (The details of the parameters of the Ti 2p peak are shown in Table S2 in Supporting Information.) On the basis of the O 1s and Ti 2p XPS spectra, it is believed that Ti−OH and Ti^{3+} species are induced by the laser irradiation of TiO_2.

The density of states (DOS) of the valence band of raw TiO_2 and TiO_2-120 were also measured by valence band XPS, the results which are shown in Figure 12D. The edges of the maximum energy of raw TiO_2 and TiO_2-120 are 3.0 and 2.6 eV, respectively. It is suggested that a blueshift (0.4 eV) of the maximum energy is induced by the laser irradiation of TiO_2, and the valence band tail states extended above the valence band maximum for 0.4 eV. In consideration of the results of the UV−vis diffuse reflectance measurement, the conduction band tail states probably extended below the conduction band minimum for 0.7 eV.

The DOS of unmodified TiO_2 and disorder-engineered TiO_2 nanospheres is shown schematically in Figure 13. The change

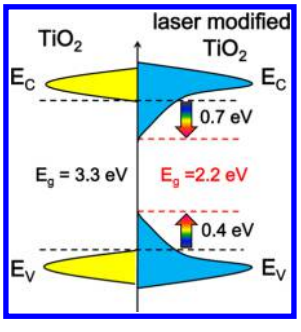

Figure 13. Schematic illustration of electronic DOS of TiO_2 before and after laser modification.

DOI: 10.1021/acsami.5b04568
ACS Appl. Mater. Interfaces 2015, 7, 16070−16077

of DOS causes the enhancement of visible light absorption of laser-modified black TiO_2 nanospheres, which is probably the reason for the relatively good photocatalytic performance of laser-modified TiO_2 under visible light. The surface lattice disorder, including Ti−H and O−H bonds, could blue-shift the valence band maximum (VBM) of anatase TiO_2 by introducing midgap states while leaving its conduction band minimum (CBM) almost unchanged.[38] Furthermore, midgap states could be introduced closely below the CBM with the formation of Ti^{3+} or oxygen vacancy.[29] In our case, band tail states were introduced around the VBM and CBM. The band tail states were probably due to the surface disorder and Ti^{3+} induced by laser irradiation.

3.5. Laser-Induced Reactive Quenching and Water-Mediated Growth of TiO_2 Nanospheres. The formation process of TiO_2 nanoparticles by laser ablation of Ti plate target in a liquid medium has been intensively studied.[39−42] It was found that these TiO_2 had no change of the absorption of the visible light. It was probably due to the different pathway of the formation of TiO_2. For the Ti plate target, according to previous studies,[39] the initial stage of interaction between pulsed-laser light and the target surface would generate a hot plasma plume over the laser spot on the metal plate, resulting in the ejection of titanium ions, atoms, and clusters from the melt surface. These species would strongly react with water molecules at the interfacial region. The chemical reaction products, such as titanium oxide or hydroxide molecules, would aggregate.

However, the formation of TiO_2 nanoparticles by laser ablation of a suspended TiO_2 solution should involve different processes. The TiO_2 nanoparticles were melting by the every single 8 ns high-energy pulse laser (instantaneous power = 4.4 MW). These initially melting TiO_2 clusters would then serve as nucleus and would rapidly be quenched in the liquid solution. These clusters must have a high fluidity so that they became spherical to reduce the surface energy. The crystalline structure of TiO_2 was broken by the laser beam at early stage. However, the anatase and rutile phase were reformed during the prolonged laser irradiation. This pathway probably benefited the formation of the disorder and the Ti^{3+} species on the surface of the TiO_2.

Ti^{3+} and oxygen vacancy could be induced in TiO_2 by high-energy particle bombardment.[36] In our case, it was probably due to the laser irradiation that a high concentration of Ti^{3+} and oxygen vacancy were induced in the surface of melting TiO_2 nanoparticles. The conduction and valence bands of TiO_2 were derived mainly from the Ti 3d and O 2p states, respectively. The high-energy laser beam ($h\nu$ = 3.49 eV) could make the electronic transition of the valence band electrons of the TiO_2, which was composed of 2p electrons of O elements. On the surface of TiO_2, O atoms donated the electrons to the Ti atoms. Therefore, Ti^{4+} accepted the electron to form the Ti^{3+}, and the O atoms could be peeled off form the surface of the TiO_2 to form the oxygen vacancies.

During the formation of the anatase and rutile phases, the oxygen vacancy and Ti^{3+} were formed on the surface of the TiO_2 nanospheres. Because the laser irradiation was carried out in a suspended solution system, the Ti^{3+} species tended to react with H_2O, and surface disorder, including Ti−OH and Ti−H, were formed. The Ti^{3+} species (oxygen vacancy) and surface disorder including Ti−OH were detected by XPS and TEM. These species could introduce band tail states in CBM and VBM and narrowed the band gap of TiO_2. TiO_2 nanospheres with absorption ability covering the full visible light spectrum were prepared by pulsed-laser ablation. The high-energy laser with s wavelength of 355 nm afforded a sufficient power to form s melting state and oxygen vacancies.

4. CONCLUSIONS

We have demonstrated a new methodology for preparing black TiO_2 nanospheres, which could be used as photocatalysts under visible light effectively. Pulsed-laser ablation of pure TiO_2 suspended in aqueous solution was carried out, and the laser-induced local high temperature and high pressure led to the formation of TiO_2 nanospheres. The laser-modified TiO_2 nanospheres could absorb a full visible light spectrum, thus exhibiting good photocatalytic performance under visible light. We believe that this enhancement of photocatalytic performance is probably because of Ti^{3+} and disorder on the surface of TiO_2 nanospheres which were introduced by pulsed-laser ablation.

■ ASSOCIATED CONTENT

Supporting Information

Luminescent spectrum of LED. Size histogram of raw TiO_2. UV−vis−NIR diffuse reflectance spectra of TiO_2. $(C/C_0)_{dark}$ versus time. $(C/C_0)_{light}$ versus irradiation time. Analysis of the SAED patterns. Parameters of the O 1s peak of XPS. Parameters of the Ti 2p peak of XPS. The Supporting Information is available free of charge on the ACS Publications website at DOI: 10.1021/acsami.5b04568.

■ AUTHOR INFORMATION

Corresponding Authors

*E-mail: zhaodx@ciomp.ac.cn.
*E-mail: liulei@ciomp.ac.cn.
*E-mail: shendz@ciomp.ac.cn.

Notes

The authors declare no competing financial interest.

■ ACKNOWLEDGMENTS

This work is supported by the National Basic Research Program of China (973 Program) under grant no. 2011CB302004, the National Science Fund for Distinguished Young Scholars 61425021, the National Natural Science Foundation of China under grant nos. 11134009, 61475153, 11174273, and 21101146, and the 100 Talents Program of the Chinese Academy of Sciences.

■ REFERENCES

(1) Fujishima, A.; Honda, K. Electrochemical Photolysis of Water at a Semiconductor Electrode. *Nature* **1972**, *238*, 37−38.
(2) Park, J. H.; Kim, S.; Bard, A. J. Novel Carbon-Doped TiO_2 Nanotube Arrays with High Aspect Ratios for Efficient Solar Water Splitting. *Nano Lett.* **2006**, *6*, 24−28.
(3) Liu, G.; Yin, L. C.; Wang, J. Q.; Niu, P.; Zhen, C.; Xie, Y. P.; Cheng, H. M. A Red Anatase TiO_2 Photocatalyst for Solar Energy Conversion. *Energy Environ. Sci.* **2012**, *5*, 9603−9610.
(4) Zhang, Z. H.; Zhang, L. B.; Hedhili, M. N.; Zhang, H. N.; Wang, P. Plasmonic Gold Nanocrystals Coupled with Photonic Crystal Seamlessly on TiO_2 Nanotube Photoelectrodes for Efficient Visible Light Photoelectrochemical Water Splitting. *Nano Lett.* **2013**, *13*, 14−20.
(5) Parrino, F.; Augugliaro, V.; Camera-Roda, G.; Loddo, V.; Lopez-Munoz, M. J.; Marquez-Alvarez, C.; Palmisano, G.; Palmisano, L.; Puma, M. A. Visible-Light-Induced Oxidation of Trans-Ferulic Acid by TiO_2 Photocatalysis. *J. Catal.* **2012**, *295*, 254−260.

DOI: 10.1021/acsami.5b04568
ACS Appl. Mater. Interfaces 2015, 7, 16070−16077

(6) Wilson, W.; Manivannan, A.; Subramanian, V. R. Heterogeneous Photocatalytic Degradation of Recalcitrant Pollutants over CdS-TiO_2 Nanotubes: Boosting Effect of TiO_2 Nanoparticles at Nanotube-CdS Interface. *Appl. Catal., A* **2012**, *441-442*, 1−9.
(7) Wang, S. L.; Qian, H. H.; Hu, Y.; Dai, W.; Zhong, Y. J.; Chen, J. F.; Hu, X. Facile One-Pot Synthesis of Uniform TiO_2-Ag Hybrid Hollow Spheres with Enhanced Photocatalytic Activity. *Dalton Trans.* **2013**, *42*, 1122−1128.
(8) Lin, J. J.; Nattestad, A.; Yu, H.; Bai, Y.; Wang, L. Z.; Dou, S. X.; Kim, J. H. Highly Connected Hierarchical Textured TiO_2 Spheres as Photoanodes for Dye-Sensitized Solar Cells. *J. Mater. Chem. A* **2014**, *2*, 8902−8909.
(9) Sun, Z. Q.; Kim, J. H.; Zhao, Y.; Bijarbooneh, F.; Malgras, V.; Lee, Y. M.; Kang, Y. M.; Dou, S. X. Rational Design of 3D Dendritic TiO_2 Nanostructures with Favorable Architectures. *J. Am. Chem. Soc.* **2011**, *133*, 19314−19317.
(10) O'Regan, B.; Gratzel, M. A Low-Cost, High-Efficiency Solar-Cell Based on Dye-Sensitized Colloidal TiO_2 Films. *Nature* **1991**, *353*, 737−740.
(11) Lee, H. U.; Lee, S. C.; Choi, S. H.; Son, B.; Lee, S. J.; Kim, H. J.; Lee, J. Highly Visible-Light Active Nanoporous TiO_2 Photocatalysts for Efficient Solar Photocatalytic Applications. *Appl. Catal., B* **2013**, *129*, 106−113.
(12) Vijay, M.; Ramachandran, K.; Ananthapadmanabhan, P. V.; Nalini, B.; Pillai, B. C.; Bondioli, F.; Manivannan, A.; Narendhirakannan, R. T. Photocatalytic Inactivation of Gram-Positive and Gram-Negative Bacteria by Reactive Plasma Processed Nanocrystalline TiO_2 Powder. *Curr. Appl. Phys.* **2013**, *13*, 510−516.
(13) Zhang, Y. Y.; Khamwannah, J.; Kim, H.; Noh, S. Y.; Yang, H. B.; Jin, S. H. Improved Dye Sensitized Solar Cell Performance in Larger Cell Size by Using TiO_2 Nanotubes. *Nanotechnology* **2013**, *24*, 045401.
(14) Gu, T. T.; Jin, R. B.; Liu, Y.; Liu, H. F.; Weng, X. L.; Wu, Z. B. Promoting Effect of Calcium Doping on the Performances of MnO_x/TiO_2 Catalysts for NO Reduction with NH_3 at Low Temperature. *Appl. Catal., B* **2013**, *129*, 30−38.
(15) Ochiai, T.; Fujishima, A. Photoelectrochemical Properties of TiO_2 Photocatalyst and Its Applications for Environmental Purification. *J. Photochem. Photobiol., C* **2012**, *13*, 247−262.
(16) Fuerte, A.; Hernandez-Alonso, M. D.; Maira, A. J.; Martinez-Arias, A.; Fernandez-Garcia, M.; Conesa, J. C.; Soria, J. Visible Light-Activated Nanosized Doped-TiO_2 Photocatalysts. *Chem. Commun.* **2001**, 2718−2719.
(17) Tada, H.; Jin, Q.; Nishijima, H.; Yamamoto, H.; Fujishima, M.; Okuoka, S.; Hattori, T.; Sumida, Y.; Kobayashi, H. Titanium(IV) Dioxide Surface-Modified with Iron Oxide as a Visible Light Photocatalyst. *Angew. Chem., Int. Ed.* **2011**, *50*, 3501−3505.
(18) Shiraishi, Y.; Sakamoto, H.; Sugano, Y.; Ichikawa, S.; Hirai, T. Pt-Cu Bimetallic Alloy Nanoparticles Supported on Anatase TiO_2: Highly Active Catalysts for Aerobic Oxidation Driven by Visible Light. *ACS Nano* **2013**, *7*, 9287−9297.
(19) Anpo, M.; Takeuchi, M. The Design and Development of Highly Reactive Titanium oxide Photocatalysts Operating under Visible Light Irradiation. *J. Catal.* **2003**, *216*, 505−516.
(20) Seh, Z. W.; Liu, S. H.; Low, M.; Zhang, S. Y.; Liu, Z. L.; Mlayah, A.; Han, M. Y. Janus Au-TiO_2 Photocatalysts with Strong Localization of Plasmonic Near-Fields for Efficient Visible-Light Hydrogen Generation. *Adv. Mater.* **2012**, *24*, 2310−2314.
(21) Asahi, R.; Morikawa, T.; Ohwaki, T.; Aoki, K.; Taga, Y. Visible-Light Photocatalysis in Nitrogen-Doped Titanium Oxides. *Science* **2001**, *293*, 269−271.
(22) Khan, S. U. M.; Al-Shahry, M.; Ingler, W. B. Efficient Photochemical Water Splitting by a Chemically Modified n-TiO_2. *Science* **2002**, *297*, 2243−2245.
(23) Varley, J. B.; Janotti, A.; Van de Walle, C. G. Mechanism of Visible-Light Photocatalysis in Nitrogen-Doped TiO_2. *Adv. Mater.* **2011**, *23*, 2343−2347.
(24) Liu, G.; Pan, J.; Yin, L. C.; Irvine, J. T. S.; Li, F.; Tan, J.; Wormald, P.; Cheng, H. M. Heteroatom-Modulated Switching of Photocatalytic Hydrogen and Oxygen Evolution Preferences of Anatase TiO_2 Microspheres. *Adv. Funct. Mater.* **2012**, *22*, 3233−3238.
(25) Zhao, J.; Chen, C.; Ma, W. Photocatalytic Degradation of Organic Pollutants under Visible Light Irradiation. *Top. Catal.* **2005**, *35*, 269−278.
(26) Wu, T. X.; Liu, G. M.; Zhao, J. C.; Hidaka, H.; Serpone, N. Photoassisted Degradation of Dye Pollutants. V. Self-Photosensitized Oxidative Transformation of Rhodamine B under Visible Light Irradiation in Aqueous TiO_2 Dispersions. *J. Phys. Chem. B* **1998**, *102*, 5845−5851.
(27) Pincella, F.; Isozaki, K.; Miki, K. A Visible Light-Driven Plasmonic Photocatalyst. *Light: Sci. Appl.* **2014**, *3*, e133.
(28) Chen, X.; Liu, L.; Yu, P. Y.; Mao, S. S. Increasing Solar Absorption for Photocatalysis with Black Hydrogenated Titanium Dioxide Nanocrystals. *Science* **2011**, *331*, 746−750.
(29) Zuo, F.; Wang, L.; Wu, T.; Zhang, Z. Y.; Borchardt, D.; Feng, P. Y. Self-Doped Ti^{3+} Enhanced Photocatalyst for Hydrogen Production under Visible Light. *J. Am. Chem. Soc.* **2010**, *132*, 11856−11857.
(30) Liu, L.; Chen, X. B. Titanium Dioxide Nanomaterials: Self-Structural Modifications. *Chem. Rev.* **2014**, *114*, 9890−9918.
(31) Zheng, Z. K.; Huang, B. B.; Lu, J. B.; Wang, Z. Y.; Qin, X. Y.; Zhang, X. Y.; Dai, Y.; Whangbo, M. H. Hydrogenated Titania: Synergy of Surface Modification and Morphology Improvement for Enhanced Photocatalytic Activity. *Chem. Commun.* **2012**, *48*, 5733−5735.
(32) Naldoni, A.; Allieta, M.; Santangelo, S.; Marelli, M.; Fabbri, F.; Cappelli, S.; Bianchi, C. L.; Psaro, R.; Del Santo, V. Effect of Nature and Location of Defects on Bandgap Narrowing in Black TiO_2 Nanoparticles. *J. Am. Chem. Soc.* **2012**, *134*, 7600−7603.
(33) Zhou, W.; Li, W.; Wang, J. Q.; Qu, Y.; Yang, Y.; Xie, Y.; Zhang, K. F.; Wang, L.; Fu, H. G.; Zhao, D. Y. Ordered Mesoporous Black TiO_2 as Highly Efficient Hydrogen Evolution Photocatalyst. *J. Am. Chem. Soc.* **2014**, *136*, 9280−9283.
(34) Li, B. B.; Zhao, Z. B.; Zhou, Q.; Meng, B.; Meng, X. T.; Qiu, J. S. Highly Efficient Low-Temperature Plasma-Assisted Modification of TiO_2 Nanosheets with Exposed {001} Facets for Enhanced Visible-Light Photocatalytic Activity. *Chem. - Eur. J.* **2014**, *20*, 14763−14770.
(35) Wang, Z.; Yang, C. Y.; Lin, T. Q.; Yin, H.; Chen, P.; Wan, D. Y.; Xu, F. F.; Huang, F. Q.; Lin, J. H.; Xie, X. M.; Jiang, M. H. H-Doped Black Titania with Very High Solar Absorption and Excellent Photocatalysis Enhanced by Localized Surface Plasmon Resonance. *Adv. Funct. Mater.* **2013**, *23*, 5444−5450.
(36) Thompson, T. L.; Yates, J. T. Surface Science Studies of the Photoactivation of TiO_2-New Photochemical Processes. *Chem. Rev.* **2006**, *106*, 4428−4453.
(37) Diebold, U. The Surface Science of Titanium Dioxide. *Surf. Sci. Rep.* **2003**, *48*, 53−229.
(38) Liu, L.; Yu, P. Y.; Chen, X.; Mao, S. S.; Shen, D. Z. Hydrogenation and Disorder in Engineered Black TiO_2. *Phys. Rev. Lett.* **2013**, *111*, 065505.
(39) Liang, C. H.; Shimizu, Y.; Sasaki, T.; Koshizaki, N. Synthesis, Characterization, and Phase Stability of Ultrafine TiO_2 Nanoparticles by Pulsed Laser Ablation in Liquid Media. *J. Mater. Res.* **2004**, *19*, 1551−1557.
(40) Tsai, M. H.; Chen, S. Y.; Shen, P. Laser Aablation Condensation of TiO_2 Particles: Effects of Laser Energy, Oxygen Flow Rate and Phase Transformation. *J. Aerosol Sci.* **2005**, *36*, 13−25.
(41) Nath, A.; Laha, S. S.; Khare, A. Effect of Focusing Conditions on Synthesis of Titanium Oxide Nanoparticles via Laser Ablation in Titanium−Water Interface. *Appl. Surf. Sci.* **2011**, *257*, 3118−3122.
(42) Alnassar, S. I.; Akman, E.; Oztoprak, B. G.; Kacar, E.; Gundogdu, O.; Khaleel, A.; Demir, A. Study of the Fragmentation Phenomena of TiO_2 Nanoparticles Produced by Femtosecond Laser Ablation in Aqueous Media. *Opt. Laser Technol.* **2013**, *51*, 17−23.

DOI: 10.1021/acsami.5b04568
ACS Appl. Mater. Interfaces 2015, 7, 16070−16077